Int. J. Multiphase Flow Vol. 15, No. 1, pp. 119–133, 1989
Printed in Great Britain.

0301-9322/89 $3.00 + 0.00

A TWO-EQUATION TURBULENCE MODEL FOR DISPERSED DILUTE CONFINED TWO-PHASE FLOWS

M. A. RIZK and S. E. ELGHOBASHI
Mechanical Engineering Department, University of California, Irvine, CA 92717, U.S.A.

(*Received* 15 *March* 1988; *in revised form* 6 *September* 1988)

Abstract—A two-equation model for low Reynolds number turbulence has been developed for dispersed dilute two-phase confined flows. The two equations describe the conservation of turbulence kinetic energy and dissipation rate of that energy for the carrier fluid. The model is based on the closure for high Reynolds number two-phase flows reported previously.

In order to validiate the proposed model, a turbulent two-phase pipe flow (air laden with spherical uniform-size particles) is predicted. The predictions of the mean flow properties of the two phases and the turbulence characteristics of the carrier phase show good agreement with the available experimental data.

Key Words: turbulence modeling, particle-laden pipe flows

1. INTRODUCTION

Modeling of confined turbulent two-phase flows is needed because a wall is ever present in most practical applications. Most of the earlier studies (e.g. Saffman 1962; Owen 1969; Choi & Chung 1983) investigated one-dimensional flows for the limiting cases of large and small relaxation times of the particles compared to the lifetime of the energetic eddies and vanishing relative velocity between the two phases. Drew (1975) studied the problem of turbulent sediment transport over the bottom of a stirring tank. His modeling approach is based on the mixing length hypothesis. The mixing length hypothesis is also used by Kramer & Depew (1972) and Choi & Chung (1983) in modeling the fully developed two-phase turbulent pipe flows. However, the mixing length model is not suitable when processes of convective and diffusive turbulent transport are important. Moreover, the model is of little use in complex flows because of the great difficulties in specifying the mixing length (Rodi 1980), even for single-phase flows.

Pourahmadi & Humphrey (1983) developed a two-equation turbulence model (k–ϵ) for two-phase confined flows. They modeled the turbulent correlations up to second order. They used the wall function approach to bridge the near-wall region in which their model cannot be applied. This is due to the fact that their model is valid only for high values of the turbulence Reynolds number. They used the universal law of the wall of single-phase flows to predict the turbulent two-phase pipe flow of Zisselmar & Molerus (1979). However, the dispersed-phase volume fractions encountered in the experiment of Zisselmar & Molerus (1979) are >0.01, which correspond to dense flow conditions. Under these conditions the use of the single-phase universal law-of-the-wall is highly questionable (see section 5.4). Even for single-phase flows, the validity of this approach is restricted to situations in which the wall functions are well tested.

The first objective of this study is to develop a second-order closure model for turbulent two-phase flows with low Reynolds number, thus providing a more reliable method for calculating wall-bounded flows than that offered by the use of either "wall–law" matching or the mixing length hypothesis. The second objective is to validate the model by comparing its predictions for a turbulent gas–solid suspension flow in a vertical pipe with the experimental data of Tsuji *et al.* (1984) and Maeda *et al.* (1980).

2. GOVERNING EQUATIONS

The governing equations for incompressible turbulent two-phase flows have been derived by Elghobashi & Abou-Arab (1983) by Reynolds decomposition and time-averaging of the instan-

taneous equations. Closure of the time-mean equations was achieved by modeling the turbulent correlations up to third order. Here we extend these equations to account for the wall effects which can be summarized as follows:

1. The total effective viscosity for fluid momentum transport is taken as the sum of the laminar and turbulent values, thus taking into account the molecular viscosity which has a dominant role in momentum transport in the wall region.
2. Saffman's lift force and the augmented particle drag due to the wall presence (Rizk & Elghobashi 1985) are included in the momentum equations of the dispersed phase.

The final set of equations is listed below:

the mean momentum equation of the carrier fluid in the x-direction,

$$\rho_1\Phi_1(U_xU_{x,x}+U_yU_{x,y})=-\Phi_1P_{,x}-\Phi_2FC_1(U_x-V_x)+\frac{1}{y^j}[\Phi_1y^j(\mu_1+\mu_t)U_{x,y}]_{,y}; \quad [1]$$

the mean momentum equation of the carrier fluid in the y-direction,

$$\rho_1\Phi_1(U_xU_{y,x}+U_yU_{y,y})=-\Phi_1P_{,y}-F\Phi_2C_2(U_y-V_y)-\tfrac{2}{3}\rho_1\frac{1}{y^j}(y^jk\Phi_1)_{,y}; \quad [2]$$

the mean momentum equation of the dispersed phase in the x-direction,

$$\rho_2\Phi_2(V_xV_{x,x}+V_yV_{x,y})=-\Phi_2P_{,x}+\Phi_2FC_1(U_x-V_x)+\frac{1}{y^j}[y^j\Phi_2(\mu_2+\mu_p)V_{x,y}]_{,y}+g_x\Phi_2(\rho_2-\rho_1); \quad [3]$$

the mean momentum equation of the dispersed phase in the y-direction,

$$\begin{aligned}\rho_2\Phi_2(V_xV_{y,x}+V_yV_{y,y})=&-\Phi_2P_{,y}+FC_2\Phi_2(U_y-V_y)\\&-\rho_2\frac{1}{y^j}\left[\tfrac{2}{3}y^jk\Phi_2\int_0^\infty\left(\frac{\Omega_1'}{\Omega_2'}+\frac{\Omega_3+\Omega_3'}{\Omega_2\Omega_2'}\right)E(\omega)\,\mathrm{d}\omega\right]_{,y}\\&+\frac{C_\ell\Phi_2\mu_1\left(\dfrac{1}{\nu_1}U_{x,y}\right)^{1/2}(U_x-V_x)}{d}+g_y\Phi_2(\rho_2-\rho_1),\end{aligned} \quad [4]$$

where $C_\ell=3.08$ (Saffman 1968);

the mean continuity equation of the carrier fluid,

$$(\Phi_1U_x)_{,x}+\frac{1}{y^j}(y^j\Phi_1U_y)_{,y}-\left[\left(\frac{\nu_t}{\sigma_{\phi_1}}\Phi_{1,x}\right)_{,x}-\frac{1}{y^j}\left(y^j\frac{\nu_t}{\sigma_{\phi_1}}\Phi_{1,y}\right)_{,y}\right]=0; \quad [5]$$

the mean continuity equation of the solid phase,

$$(\Phi_2V_x)_{,x}+\frac{1}{y^j}(y^j\Phi_2V_y)_{,y}-\left[\left(\frac{\nu_t}{\sigma_{\phi_2}}\Phi_{2,x}\right)_{,x}-\frac{1}{y^j}\left(y^j\frac{\nu_t}{\sigma_{\phi_2}}\Phi_{2,y}\right)_{,y}\right]=0; \quad [6]$$

and

the mean global continuity equation,

$$\Phi_1+\Phi_2=1; \quad [7]$$

where $j=0$ for plane flows, $j=1$ for axisymmetric flows,

$$\Omega_2=\frac{1}{\beta^2}\left(\frac{\omega}{\alpha}\right)^2+\frac{\sqrt{6}}{\beta}\left(\frac{\omega}{\alpha}\right)^{3/2}+3\left(\frac{\omega}{\alpha}\right)+C_1\sqrt{6}\left(\frac{\omega}{\alpha}\right)^{1/2}+C_1^2, \quad [8]$$

$$\Omega_1'=\left(\frac{\omega}{\alpha}\right)^2+\sqrt{6}\left(\frac{\omega}{\alpha}\right)^{3/2}+3\left(\frac{\omega}{\alpha}\right)+C_2\sqrt{6}\left(\frac{\omega}{\alpha}\right)^{1/2}+C_2^2, \quad [9]$$

$$\Omega_2' = \frac{1}{\beta^2}\left(\frac{\omega}{\alpha}\right)^2 + \frac{\sqrt{6}}{\beta}\left(\frac{\omega}{\alpha}\right)^{3/2} + 3\left(\frac{\omega}{\alpha}\right) + C_2\sqrt{6}\left(\frac{\omega}{\alpha}\right)^{1/2} + C_2^2, \quad [10]$$

$$\Omega_3' = \gamma\theta\left[\left[\frac{(1-\beta)}{\beta}\left\{\left[6 + 2\left(C_1 + \frac{C_2}{\beta}\right)\right]\left(\frac{\omega}{\alpha}\right)^2 + \sqrt{6}(C_1 + C_2)\left(\frac{\omega}{\alpha}\right)^{3/2} + \sqrt{6}\,\frac{(1+\beta)}{\beta}\left(\frac{\omega}{\alpha}\right)^{5/2}\right\}\right], \quad [11]$$

$$\Omega_3 = \gamma^2\theta^2\Omega_R, \quad [12]$$

$$\Omega_R = \left(\frac{1-\beta}{\beta}\,\frac{\omega}{\alpha}\right)^2, \quad [13]$$

$$\alpha = \frac{12\nu_1}{d^2}, \quad [14]$$

$$\beta = \frac{3\rho_1}{(2\rho_2 + \rho_1)}, \quad [15]$$

$$\theta = \frac{d}{\eta}, \quad [16]$$

η is the Kolmogoroff length scale,

$$\eta = \left(\frac{\nu^3}{\epsilon}\right)^{1/4} \quad [17]$$

and

$$\gamma = \mathrm{K}/3\pi. \quad [18]$$

In the above equations, x is the coordinate parallel to the wall and y is the coordinate normal to it; U_i and V_i are the mean velocities of the fluid and particles, respectively, in the i-direction; d is the particle diameter; F is the momentum exchange coefficient; ρ is the density; Φ is the volume fraction; and the subscripts 1 and 2 denote the fluid and particles, respectively; g is the gravitational acceleration.

C_1 and C_2 are correction factors which account for the effect of the wall on the Stokesian drag. Near the wall the fluid decelerates in order to satisfy the no-slip condition at the wall while the particles slip by. Accordingly, the relative velocity between the particles and the fluid increases, thus augmenting the drag force of the particles. Here we follow Rizk & Elghobashi (1985) in evaluating C_1 and C_2. We adopt Faxen's (1923) expression for C_1 and Brenner's (1961) and Maude's (1961) expressions for C_2. These expressions read as follows:

$$C_1 = \left[1 - \frac{9}{16}\left(\frac{d}{2y}\right) + \frac{1}{8}\left(\frac{d}{2y}\right)^3 - \frac{45}{256}\left(\frac{d}{2y}\right)^4 - \frac{1}{16}\left(\frac{d}{2y}\right)^5\right]^{-1} \quad [19]$$

and

$$C_2 = 1 + \frac{9}{8}\left(\frac{d}{2y}\right) + \left(\frac{9}{16}\frac{d}{y}\right)^2. \quad [20]$$

For example, setting $(d/y) = 0.5$ in [19] and [20] results in increasing the drag forces in the directions parallel and normal to the wall by 20 and 30% respectively, above their values in unbounded flow.

The term containing C_ℓ on the r.h.s. of [4] is the volume-averaged counterpart of Saffman's lift force, F_ℓ, acting on the dispersed phase in any control volume, given by

$$F_\ell = \mathrm{K}\mu_1 d^2\left(\frac{1}{\nu_1}\,U_{x,y}\right)^{1/2}(U_x - V_x), \quad [21]$$

where K is a constant obtained via numerical integration whose value was corrected from 20.3 to 1.615 by Saffman (1968). This term shows that if the dispersed phase leads the fluid in the x-direction, the lift force will be negative and tend to drive the particles toward the wall. Although Saffman's lift force has been derived for a sphere suspended in a free uniform shear flow, it is used in this study for the following reasons: (i) in the vicinity of the wall, the particle is subjected to a uniform shear due to the linearity of the fluid velocity distribution there; and (ii) the direction of the lift force observed experimentally for both neutrally buoyant and nonneutrally buoyant spheres suspended in wall-bounded flows has been correctly predicted by Saffman's expression (see Brenner 1961; Theodore 1964).

It should be noted that we have seven unknowns (U_x, U_y, V_x, V_y, P, Φ_1, and Φ_2) and seven equations, [1]–[7]. So, the equation set can be solved numerically once the auxiliary quantities (ν_t, ν_p, ν_2, σ_{ϕ_2} and F) are available together with appropriate boundary conditions. The calculation of these quantities will be discussed in section 4.

3. THE LOW REYNOLDS NUMBER TURBULENCE MODEL

The high Reynolds number turbulence model developed by Elghobashi & Abou-Arab (1983) for free shear flows is modified as follows to account for wall effects. Thus, the viscous diffusion of k and ϵ is included. The sources and sinks of the ϵ equation and likewise the eddy viscosity of the carrier fluid are made functions of the local Reynolds number of turbulence (Jones & Launder 1972). Terms in the exact equations of k and ϵ which account for anisotropic dissipation (Jones & Launder 1972) are included. The correlations which represent the interaction between the particles and fluid turbulence are remodeled to account for the presence of the wall.

The final form of the turbulence model equations used in this study (Rizk 1985) are given below:

turbulence kinetic energy, k

$$\rho_1\Phi_1(U_x k_{,x} + U_y k_{,y}) = \rho_1\Phi_1 \frac{1}{y^j}\left[y^j \frac{(\nu_t + \nu_1)}{\sigma_k} k_{,y}\right]_{,y} + (\rho_1\Phi_1 \nu_t U_{x,y} U_{x,y}) - \rho_1\Phi_1\epsilon$$

convection — diffusion — G

$$-\left[\left[F\Phi_2\left\{1 - \int_0^\infty \left[\frac{2}{3}\frac{(\Omega_1 - \Omega_R)}{\Omega_2} + \frac{1}{3}\left(\frac{\Omega_1' - \Omega_R}{\Omega_2'} + \frac{\Omega_3' + \Omega_4}{\Omega_2\Omega_2'}\right)\right]\right\}E(\omega)\,d\omega\right] - \left(\rho_1\Phi_1\frac{2\nu_1 k}{y^2}\right); \quad [22]$$

ϵ_e — ϵ_w

and

turbulence energy dissipation rate, ϵ

$$\rho_1\Phi_1(U_x\epsilon_x + U_y\epsilon_{,y}) = \rho_1\Phi_1\frac{1}{y^j}\left[y^j\frac{(\nu_t + \nu_1)}{\sigma_\epsilon}\epsilon_{,y}\right]_{,y} + c_{\epsilon_1}G\frac{\epsilon}{k} - \rho_1\Phi_1 c_{\epsilon_2} f_2\frac{\epsilon^2}{k} - c_{\epsilon_3}\frac{\epsilon}{k}\epsilon_e - \frac{\epsilon}{k}f_w\epsilon_w. \quad [23]$$

It should be noted that [22] and [23] do not contain the terms representing third-order correlations. The same applies to the mean momentum equations [1]–[4]. This was based on careful examination of the magnitudes of these terms in the flow considered here, which showed that these terms can be neglected.

The quantities μ_t, Ω_1 and Ω_4 are given by

$$\mu_t = c_\mu f_\mu \frac{\rho_1 k^2}{\epsilon}, \quad [24]$$

$$\Omega_1 = \left(\frac{\omega}{\alpha}\right)^2 + \sqrt{6}\left(\frac{\omega}{\alpha}\right)^{3/2} + 3\left(\frac{\omega}{\alpha}\right) + C_1\sqrt{6}\left(\frac{\omega}{\alpha}\right)^{1/2} + C_1^2 \quad [25]$$

and

$$\Omega_4 = \gamma\theta\Omega_R\left[2C_1 + \sqrt{6}\left(\frac{\omega}{\alpha}\right)^{1/2}\right]. \quad [26]$$

The Lagrangian frequency function of the carrier fluid, $E(\omega)$, is, in general, affected by the presence of the dispersed phase. In the low frequency range (inertial subrange), the modulation of $E(\omega)$ by the dispersed phase can be neglected (Al Taweel & Landau 1977). Thus, in the present work the Lagrangian frequency function is given by (Hinze 1975)

$$E(\omega) = \left(\frac{2}{\pi}\right)\frac{T_L}{(1+\omega^2 T_L^2)}, \qquad [27]$$

where ω ranges from 1 to 10^4 (s^{-1}) and T_L, the local Lagrangian integral time scale, is calculated from (Hinze 1975)

$$T_L = 0.2\frac{k}{\epsilon}. \qquad [28]$$

The influence of Reynolds number mentioned above is introduced via the three functions f_2, f_w and f_μ which are assigned the following forms (Jones & Launder 1972; Chien 1980) and appear in [23] and [24]:

$$f_2 = 1 - 0.22\exp\left[-\left(\frac{\nu_t}{6\nu_l}\right)^2\right], \qquad [29]$$

$$f_w = \exp(-0.5Y^+) \qquad [30]$$

and

$$f_\mu = 1 - \exp(-0.0115Y^+), \qquad [31]$$

where $Y^+ = (U_\tau y)/\nu_l$ and U_τ is the friction velocity.

ϵ_w is needed to balance the molecular diffusion of k which is finite at $y = 0$. Chien (1980) used a Taylor series expansion for the fluctuating velocity components in the limit at $y = 0$,

$$\epsilon_w = 2\nu_l\frac{k}{y^2}. \qquad [32]$$

4. CALCULATION OF THE AUXILIARY QUANTITIES

In this section we calculate the dispersed-phase transport parameters, σ_{ϕ_2}, ν_p, ν_2 and the momentum exchange coefficients F.

4.1. Turbulent Schmidt number of the dispersed phase, σ_{ϕ_2}

The turbulent diffusivity of solid particles D_p, is evaluated by introducing the dispersed-phase Schmidt number σ_{ϕ_2}, defined as

$$\sigma_{\phi_2} = \frac{\nu_t}{D_p}. \qquad [33]$$

Gouesbet *et al.* (1983) developed the following semi-empirical equation for σ_{ϕ_2}diffusivity along the lines of Csanady (1963):

$$\sigma_{\phi_2} = \left[1 + \tfrac{3}{2}C_\beta\frac{(V_i - U_i)^2}{k}\right]^{1/2}. \qquad [34]$$

The empirical constant C_β is determined through optimization to obtain good agreement with the particle dispersion data of Snyder & Lumley (1971) and Wells (1982). The value of C_β is found to be 0.85. Equation [34] is used in this study for the particle Schmidt number, σ_{ϕ_2}.

4.2. Turbulent kinematic viscosity of the dispersed phase, ν_p

Experimental evidence (cf. Modarress *et al.* 1982, 1983) suggests that the kinematic eddy viscosity of the dispersed phase,ν_p, is different from the eddy diffusivity of the particles, D_p. In this study, ν_p is calculated by introducing another Schmidt number, σ_p,

$$\sigma_p = \frac{\nu_p}{D_p}. \qquad [35]$$

The value of σ_p is about 1.5. This value was determined (Rizk 1985) by computer optimization to achieve good agreement between the predicted and measured mean velocity profiles of the dispersed phase in a round gaseous jet laden with spherical uniform-size solid particles and the corresponding experimental data of Modarress *et al.* (1982, 1983).

4.3. Laminar kinematic viscosity of the dispersed phase, ν_2

On the molecular level, collision between the particles and fluid molecules is the main mechanisms of exchanging momentum between the particles and the fluid. This interaction between the particles and the fluid enhances the momentum transfer between the adjacent layers of the fluid. We evaluate ν_2 by assuming that $\nu_l/\nu_t = \nu_2/\nu_p$ (Choi & Chung 1983):

$$\frac{\nu_2}{\nu_p} = \frac{\nu_l}{\nu_t} \qquad [36]$$

and

$$\frac{\nu_l}{\nu_2} = \frac{\nu_t}{\nu_p} = \frac{\nu_t}{\sigma_p D_p}. \qquad [37]$$

With the aid of [33] we can write

$$\frac{\nu_l}{\nu_2} = \frac{\nu_t}{\nu_p} = \frac{\sigma_{\phi_2}}{\sigma_p}. \qquad [38]$$

4.4. The momentum exchange coefficient, F

The momentum exchange coefficient is given by

$$F = Q\left(18\frac{\mu_l}{d^2}\right), \qquad [39]$$

where Q is a correction factor for the Stokes' drag law which depends on the particle Reynolds number and can be obtained from the standard drag curve of steady flow around a sphere (Clift *et al.* 1978).

5. MODEL VALIDATION

5.1. The flow considered

The flow selected to validate our model is the turbulent two-phase pipe flow (see figure 1) for which some experimental data are available. We compare our predictions with the experimental data of Tsuji *et al.* (1984) and Maeda *et al.* (1980). Table 1 lists the experimental conditions for the test cases used in the comparison. In both experiments, a laser-Doppler velocimeter (LDV) was used to measure the velocities of air and solid particles in a vertical pipe two-phase flow.

It should be mentioned that neither Tsuji *et al.* (1984) nor Maeda *et al.* (1980) made measurements in the wall region ($Y^+ < 50$).

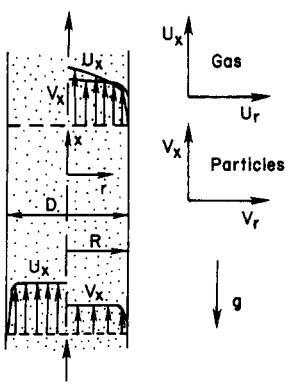

Figure 1. Flow schematic.

Table 1. The experimental test cases used for model validation

Investigaor	Re	d (μm)	$\frac{\rho_2}{\rho_1}$	Φ_0	Two-phase system
Tsuji *et al.* (1984)	2.3×10^4 (case 1)	200	866	0.5	Polystyrene particles/air
				0.9	
	3.3×10^4 (case 2)			1.3	
				1	
				2.1	
Maeda *et al.* (1980)	2×10^4 (case 3)	45	2200	0.3	Glass particles/air
		136		0.3	
				0.54	

Zisselmar & Molerus (1979) studied the modulation of fluid turbulence due to the presence of solid particles in a dispersed solid–liquid turbulent pipe flow. They reported measurements of the turbulence intensities up to a wall distance of $Y^+ = 13.4$. However, the dispersed-phase volume fractions in their experiment were >0.01, which far exceeds the dilute regime limit of 0.004, thus indicating dense two-phase flow conditions. For such densely-laden flows the momentum exchange mechanisms are not limited to gas–particle interactions but also to particle–particle interactions. Therefore, their data are not used in the validation of our model. In the absence of experimental data in the wall region for dilute two-phase flows and in order to show the effects of the solid particles on the law of the wall, we consider a hypothetical two-phase flow in which the dispersed phase consists of spherical particles of uniform size ($d = 45$ μm).

The inlet conditions of the carrier fluid (air) flow are identical to those of the single-phase pipe flow of Laufer (1954). Therefore any deviations in the fluid velocity field from that measured by Laufer in the wall region will be due to presence of the particles in air flow.

In order to study the effect of the particle material density on the flow we examined two cases. In the first, the ratio of the particle density to that of the fluid, $\rho_2/\rho_1 = 100$; and in the second case, $\rho_2/\rho_1 = 2000$.

5.2. *Boundary conditions*

The parabolic flow considered here requires the prescription of three boundary conditions for each dependent variable.

The inlet profiles of the mean velocity and concentration of the dispersed phase were assumed uniform. We insured that these inlet profiles satisfy the specified mass loading ratio of the experiment. The inlet k profile was assumed similar to that measured by Laufer (1954). The starting condition for the rate of dissipation ϵ was generated from the following formula (Launder & Spalding 1972):

$$\epsilon = C_\mu^{0.75} \frac{k^{1.5}}{l}, \qquad [40]$$

where l is the integral turbulence length scale which equals $0.1R$, where R is the pipe radius. In general the inlet conditions exerted a minor influence on the results far downstream in the fully developed region.

At the axis of symmetry ($r = 0$) all the radial gradients are set to zero, in addition to the vanishing radial velocity for each phase.

At the solid walls, $y = 0$, the boundary conditions are

$$u = k = \epsilon = 0 \qquad [41]$$

and

$$\frac{d\Phi_2}{\partial r} = 0. \qquad [42]$$

In the case of fluid–particle flows, the particles may be in slip motion at the wall while the fluid satisfies the no-slip condition. Consequently, the particles and carrier phase do not satisfy the same wall boundary conditions. When there is no net deposition (a situation which can be achieved when

the pipe is vertical and there are no electrostatic forces) of the particles, the normal velocity component at the wall vanishes, even when field forces are present. Accordingly, in this study, the normal velocity component of the dispersed phase will be assigned a zero value at the wall. The boundary condition for the tangential velocity of the dispersed phase at the wall for a fully developed pipe flow is obtained from the mean momentum equations of the carrier fluid and the dispersed phase in the x-direction by neglecting the terms containing volume-fraction fluctuations. The result is

$$V_{x,r}|_w = \frac{1}{\mu_2 \Phi_{2w}} \left\{ \frac{R}{2} [P_{w,x} - \Phi_{2w}(\rho_2 - \rho_1)g] - \Phi_{1w} \mu_1 U_{x,r}|_w \right\}. \quad [43]$$

5.3. Numerical solution procedure

The numerical method used in this work is a modified version of the marching integration procedure of Spalding (1979). The modifications include the treatment of the turbulent correlations existing in the continuity and momentum equations of the two phases. Forty-four cross-stream grid nodes were used to obtain grid-independent solutions and, for an accurate representation of the large gradients in the vicinity of the wall, roughly one-fourth of those were located with $Y^+ < 50$. For the case of Laufer's single-phase flow ($\mathrm{Re} = 5 \times 10^4$) only, 52 cross-stream grid nodes were used. The first grid point was normally located at $Y^+ = 1$ and it was insured that this value did not exceed $Y^+ = 2$ in the course of the computation.

The streamwise step size was taken as five sublayer thicknesses.

More details about the numerical solution are given in Rizk (1985).

5.4. Results and discussion

The values of the new constants in the turbulance model, namely σ_{ϕ_1} and c_{ϵ_3} were determined previously by Elghobashi *et al.* (1984) for jet flows and have been reoptimized here for turbulent two-phase pipe flows. The values of the coefficients appearing in [22]–[24] are listed in table 2.

As shown in table 2, the value of σ_{ϕ_1} was kept the same as proposed by Elghobashi *et al.* (1984). The value of σ_{ϵ_3} ($=2.0$) was determined through a parametric study to achieve the best possible agreement with the experimental data. This value is greater than that (1.3) reported by Elghobashi *et al.* (1984) for jet flows. The dependence of the value of c_{ϵ_3} on the type of flow, i.e. jet or pipe, suggests that c_{ϵ_3} may be a function of local flow conditions rather than a constant. A sensitivity analysis was carried out to address the impact of the variations of σ_{ϕ_1} and c_{ϵ_3} on the results. A 15% change in c_{ϵ_3} resulted in a maximum change of about 3% in the mean velocity profiles and about 7% in the turbulence quantities. A 20% change in the value of σ_{ϕ_1} resulted in a maximum change of 2% in the results.

The results consist of two main parts. The first contains a comparison of the model predictions with the experimental data of Tsuji *et al.* (1984) and Maeda *et al.* (1980). The second presents the model predictions in the wall region for the hypothetical two-phase flow described above.

Figure 2 compares the calculated and measured values of fully developed mean longitudinal velocities for the fluid and dispersed phase for case 1 mean longitudinal velocities for the fluid and dispersed phase for case 1 ($d = 200\,\mu\mathrm{m}$, $\rho_2/\rho_1 = 866$, $\mathrm{Re} = 2.3 \times 10^4$) and $\Phi_0 = 1.3$. The velocity of the particles is smaller than the air velocity over 90% of the cross section; it becomes larger than the air velocity near the wall because the air flow is subject to the no-slip condition at the wall while the dispersed phase slips by. Therefore, in a vertical pipe flow, there must be a location where the sign of relative velocity between both phases changes. The figure shows reasonable agreement between the predictions and experimental data.

The effect of the mass loading ratio Φ_0 on the air streamwise mean velocity profiles is shown in figures 3 and 4 for case 1 ($d = 200\,\mu\mathrm{m}$, $\rho_2/\rho_1 = 866$, $\mathrm{Re} = 2.3 \times 10^4$) and case 3 ($d = 136\,\mu\mathrm{m}$,

Table 2. Coefficients of the turbulence model

σ_k	σ_ϵ	c_μ	$c_{\epsilon 1}$	$c_{\epsilon 2}$	$\sigma_{\phi 1}$	$c_{\epsilon 3}$
1.0	1.3	0.09	1.35	1.8	1.0	2.0

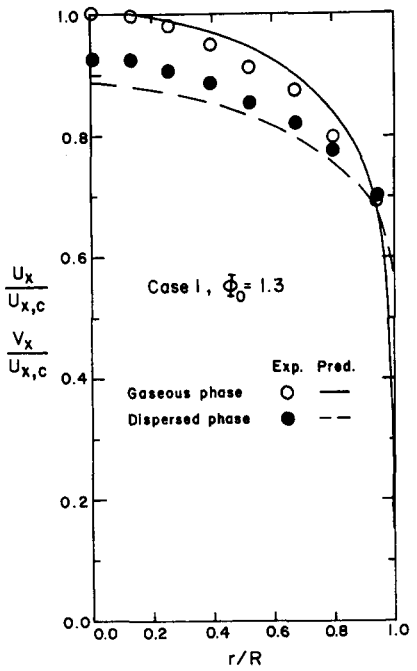

Figure 2. Normalized mean velocity profiles for case 1 and $\Phi_0 = 1.3$.

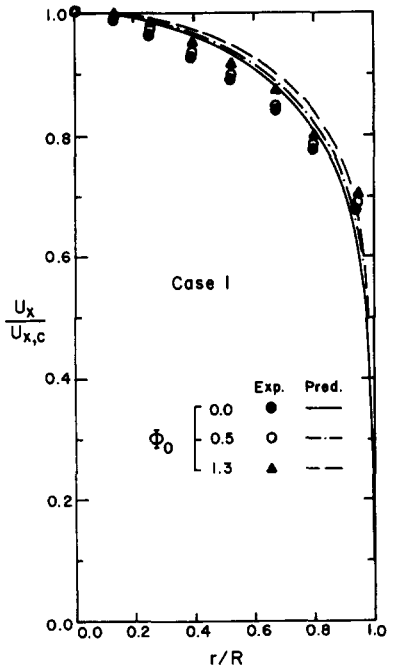

Figure 3. Effect of the mass loading ratio on the carrier phase normalized mean velocity profiles for case 1.

$\rho_2/\rho_1 = 2200$, $\mathrm{Re} = 2 \times 10^4$). These figures indicate that the addition of the solid particles flattens the air velocity profile in the core of the pipe but steepens it in the region near the wall; this effect is augmented with increasing the mass loading ratio Φ_0. Since the velocity of the dispersed phase is higher than that of the air in the wall region due to their different boundary conditions at the wall, the dispersed phase acts as a source of momentum for the air which will be accelerated there. The air then decelerates in the core region to satisfy its conservation of mass and also due to the

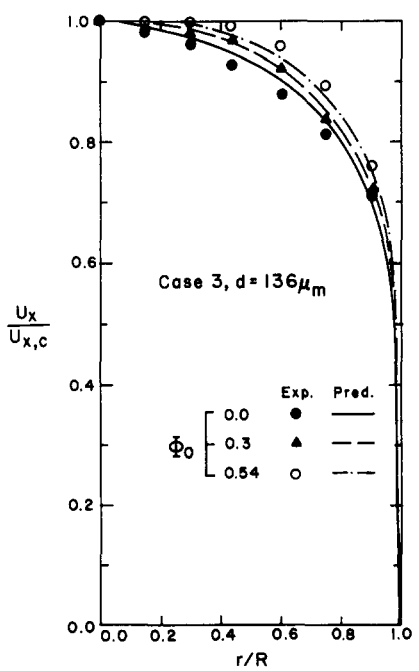

Figure 4. Effect of the mass loading ratio on the carrier phase normalized mean velocity profiles for case 3 and $d = 136\ \mu$m.

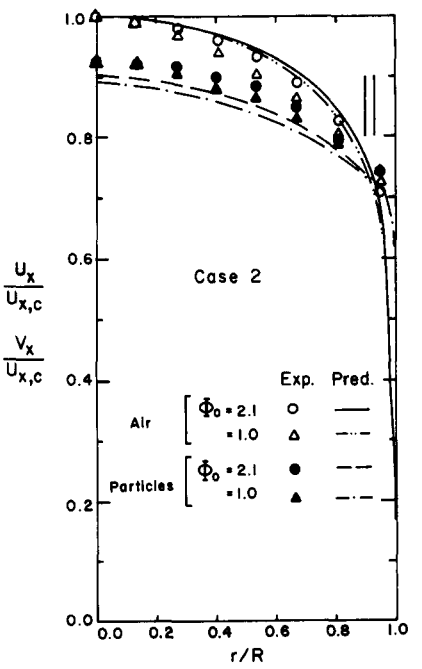

Figure 5. Normalized mean velocity profiles for case 2.

particles drag, with the net result of flattening the air velocity profile in the core region and steepening it in the wall region. Increasing the mass loading ratio enhanced the effectiveness of momentum transfer from the dispersed phase to the air in the wall region and thus increases the flatness of the air velocity profile in the core region. The agreement between the predictions and the experimental data is good (maximum error $\simeq 6\%$).

The effect of the mass loading ratio on the location at which the slip velocity vanishes is demonstrated in figure 5, which shows that this location moves away from the wall with decreasing the loading ratio. This may be explained as follows: increasing the mass loading ratio increases the flatness of the air velocity profile, whereas the dispersed-phase mean velocity profile is not affected significantly; thus, the location of vanishing relative velocity approaches the wall by increasing the mass loading ratio.

The measured and predicted mean velocity profiles for case 3 ($d = 45$, $136\,\mu$m, $\Phi_0 = 0.3$, $\mathrm{Re} = 2 \times 10^4$) are shown in figure 6. This figure shows that the effect of small-size particles on the flatness of the air velocity profile is more marked than that of larger particles for the same loading ratio. This is attributed to the interphase surface area acted on by viscous drag. This surface area for $45\,\mu$m particles is about three times that for $136\,\mu$m particles. Furthermore, the smaller the particle size, the less is the value of the relative velocity. As a result, the change in sign of the relative velocity occurs at larger distance from the wall for small particles than for larger particles. The agreement between the measured and predicted mean fluid velocities is very good. The maximum discrepancy in the mean solid-phase velocities is about 8%, which is well within the bounds of experimental error (indicated in the figure by the two crosses).

The influence of the mass loading ratio Φ_0 on the fluid turbulent intensity and the turbulent shear stress is shown in figures 7 and 8, respectively. Both the measurements and predictions show that increasing Φ_0 reduces the intensity $\sqrt{\overline{u_x^2}}/U_{x,c}$ which can be lower than the single-phase value by as much as 38% for $\Phi_0 = 1.3$ at the pipe centerline. The predicted reduction of $\sqrt{\overline{u_x^2}}/U_{x,c}$ is attributed mainly to the effect of the new dissipation term, ϵ_e, in [22]. This conclusion is based on the result of computations performed using the complete set of governing equations [1]–[7] for the two phases together with the k and ϵ equations of single-phase flow (i.e. [22] and [23] without the ϵ_e terms) for $\Phi_0 = 1.3$. The predicted $\sqrt{\overline{u_x^2}}/U_{x,c}$ from these equations is plotted in figure 7. It is seen that the reduction in the centerline turbulence intensity, as compared to that of the single-phase value, is only half that measured and predicted by the two-phase k–ϵ model.

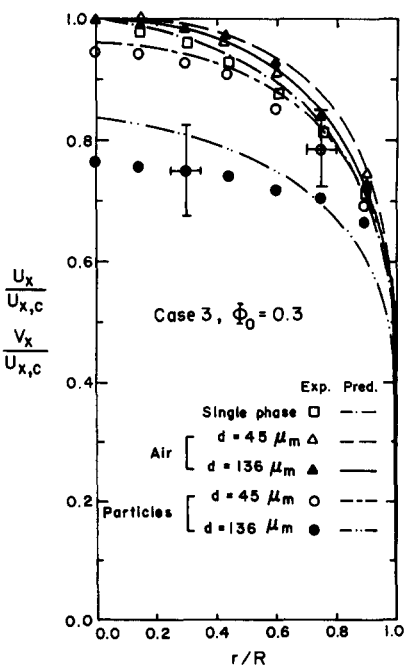

Figure 6. Normalized mean velocity profiles for case 3 and $\Phi_0 = 0.3$.

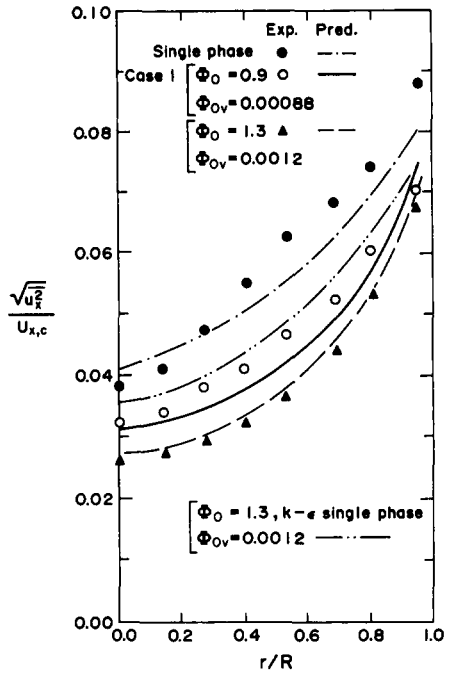

Figure 7. Turbulence intensity profiles for case 1 and different mass loading ratios.

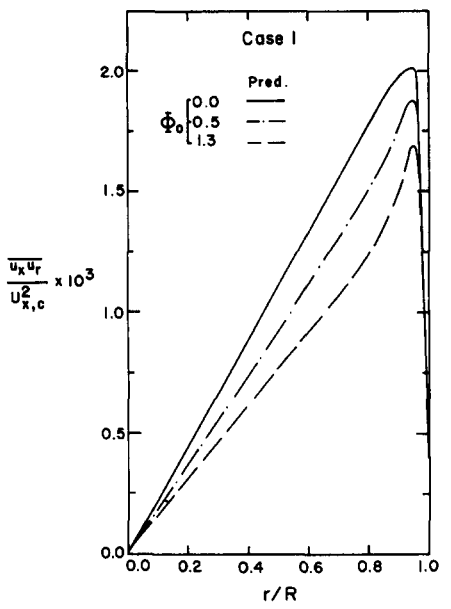

Figure 8. Turbulence shear stress profiles for case 1 and different mass loading ratios.

Increasing Φ_0 results in increasing the number of particles and hence their contribution to the sink of k. Figure 8 shows that the fluid turbulent shear stress decreases with increasing Φ_0. At the wall the viscous shear stress is much greater than the turbulent stress. Figures 3 and 4 indicate that the mean velocity gradient at the wall, and hence the wall shear stress, increase by increasing Φ_0. This fact is manifested in figure 9 which displays the percentage change of the wall shear stress τ_w from the single-phase value vs the mass loading ratio Φ_0 for case 1. It is seen that the wall shear stress increases due to the addition of the particles and consequently the pressure drop in the pipe increases. From a design point of view, this is an important result because it indicates that for the same mean-flow Reynolds number, a more powerful pump is needed for pumping gas–solid flow than that required for pumping gas alone.

Figures 10–15 show the predicted profiles of the fluid turbulence kinetic energy, turbulent shear stress and streamwise mean velocity in the wall region of the hypothetical two-phase flow described at the end of section 5.1 above. The single-phase data of Laufer (1954) are also plotted in these figures to show the deviations, due to the presence of particles in our flow, of our turbulence properties from those of Laufer's.

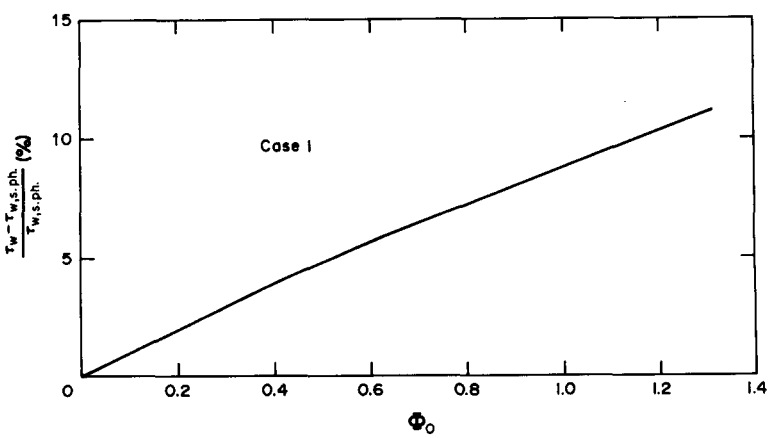

Figure 9. Variation of the wall shear stress with the mass loading ratio for case 1.

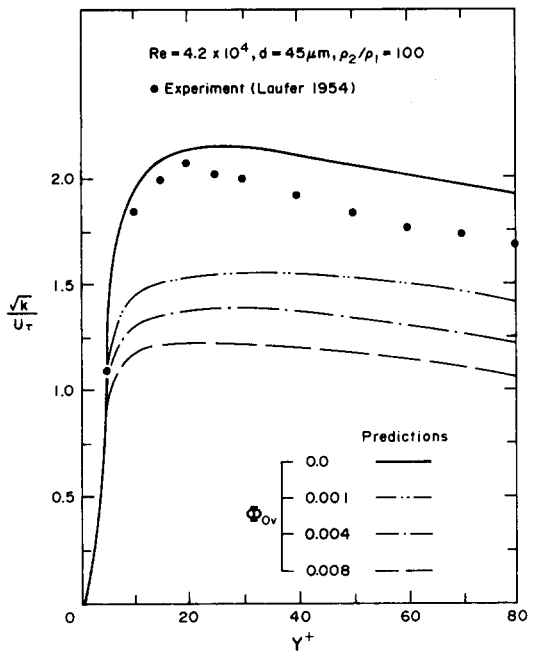

Figure 10. $\sqrt{k}/U_\tau$ profiles near the wall for $d = 45\,\mu$m, $\rho_2/\rho_1 = 100$ and different volumetric loading ratios, including the single-phase pipe flow of Laufer (1954).

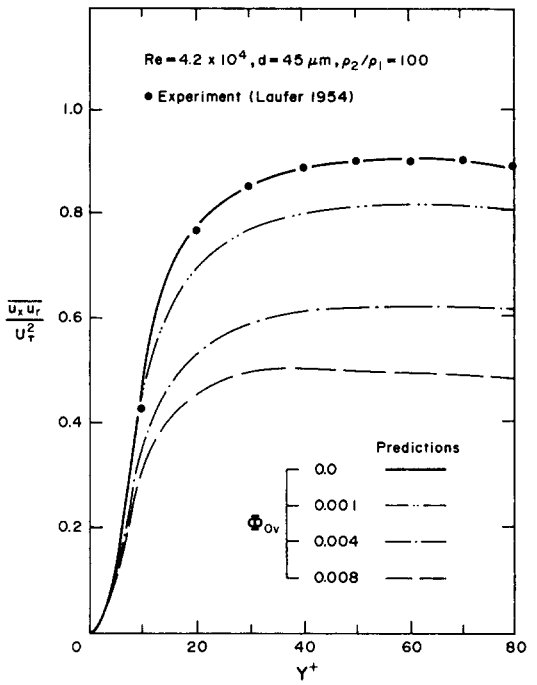

Figure 11. Normalized turbulent shear stress profiles near the wall for $d = 45\,\mu$m, $\rho_2/\rho_1 = 100$ and different volumetric loading ratios, including the single-phase pipe flow of Laufer (1954).

The diameter of the particles is 45 μm in the two cases studied. In case 1, $\rho_2/\rho_1 = 100$ which corresponds to snow particles in air. In case 2, $\rho_2/\rho_1 = 2000$ which corresponds to sand particles in air. Figure 10 shows the profiles of $\sqrt{k}/U_\tau$ in the wall region ($0 < Y^+ \leqslant 80$) for different volumetric loading ratios Φ_{0v}. The reduction of $\sqrt{k}/U_\tau$ and $\overline{u_x u_r}/U_\tau^2$ with increasing volumetric

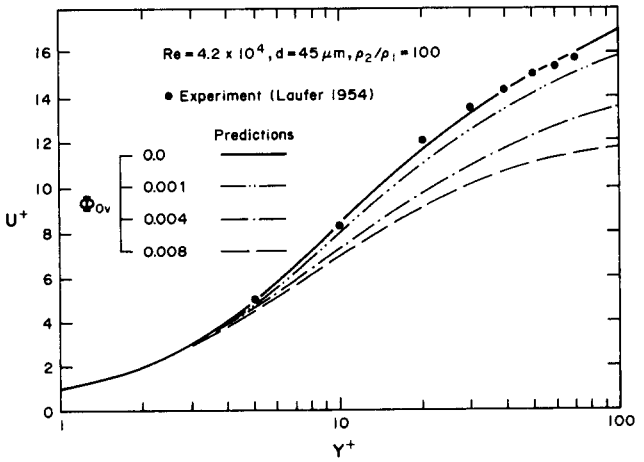

Figure 12. Normalized mean velocity profiles near the wall for $d = 45\,\mu$m, $\rho_2/\rho_1 = 100$ and different volumetric loading ratios, including the single-phase pipe flow of Laufer (1954).

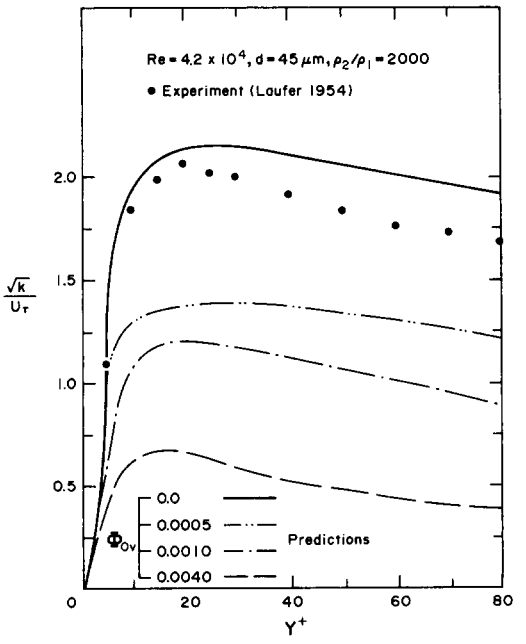

Figure 13. $\sqrt{k}/U_\tau$ profiles near the wall for $d = 45\,\mu$m, $\rho_2/\rho_1 = 2000$ and different volumetric loading ratios, including the single-phase pipe flow of Laufer (1954).

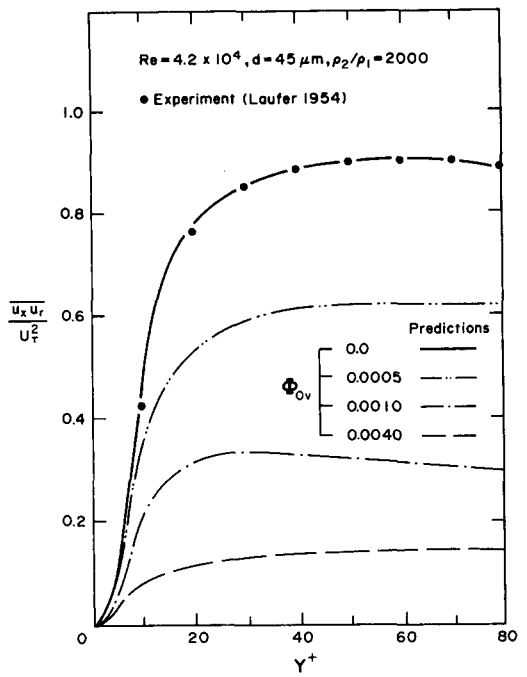

Figure 14. Normalized turbulent shear stress profiles near the wall for $d = 45\ \mu m$, $\rho_2/\rho_1 = 2000$ and different volumetric loading ratios, including the single-phase pipe flow of Laufer (1954).

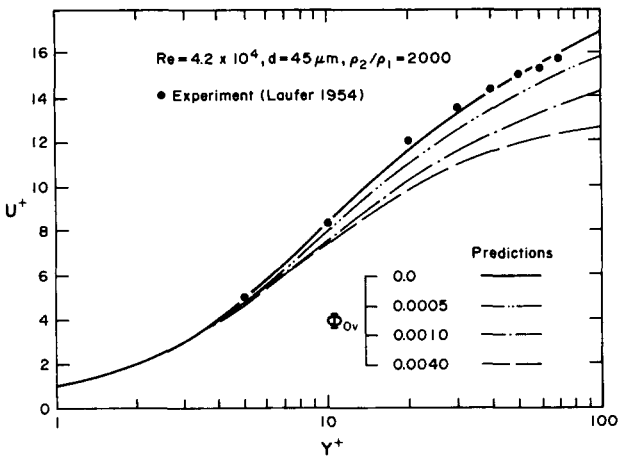

Figure 15. Normalized mean velocity profiles near the wall for $d = 45\ \mu m$, $\rho_2/\rho_1 = 2000$ and different volumetric loading ratios, including the single-phase pipe flow of Laufer (1954).

loading ratio, Φ_{0v}, can be explained in the same manner as for figures 7 and 8. Figures 12 and 15 show the effect of increasing Φ_{0v} on the law-of-the-wall. Increasing Φ_{0v} results in reducing $U^+ (= U_x/U_\tau)$. Increasing Φ_{ov} increases the magnitude of the axial pressure gradient dP/dx, and consequently U_τ, which results in lowering U^+.

Comparison of figures 10–12 with those in figures 13–15 indicates that, for the same volumetric loading ratio, the higher density ratio (ρ_2/ρ_1) has a more pronounced effect on the turbulence characteristics than the smaller density ratio. When the law-of-the-wall is used in the computation, the first grid point near the wall is located at about $Y^+ = 30$. Figure 15 shows that the deviations of the velocity profile from that of the single phase at $Y^+ = 30$ for $\Phi_{0v} = 0.0005$, 0.001 and 0.004 are about 4, 12 and 16%, respectively. The deviations from the single-phase values for k and $\overline{u_x u_r}$ are much larger than those encountered in the velocity profiles. Based on these results, the law-of-the-wall should not be used for volumetric loading ratios >0.0005. The error in specifying the velocity boundary condition based on the single-phase law-of-the-wall increases with increasing Φ_{0v}.

6. CONCLUDING REMARKS

The paper presented a low Reynolds number turbulence model for confined two-phase flows in which the local value of the turbulent viscosity is determined from the solution of transport equations for the turbulence kinetic energy and its dissipation rate. The proposed model accounts for the interaction between the two phases and the wall and its influence on turbulence structure. Comparison of the predictions with experimental data indicates that the new turbulence model predicts the significant effects of the solid particles on the pipe flow. It has been found that, in this flow, third-order correlations and the second-order correlations including volume-fraction fluctuations, except those in the continuity equations, have negligible effects on the flow. This study shows that the addition of solid particles to a turbulent vertical pipe flow affects the flow in the following manner:

1. The air leads the particles in the core region and lags behind the particles near the wall. This behavior is due to the fact that the fluid does not slip at the wall

where particles do. Consequently, the air mean velocity profile is flatter in the core of the pipe and steeper near the wall; this effect is augmented by increasing the mass loading ratio or decreasing the particle size.

2. The mean relative velocity between the gas and particles is mainly a function of the size and material density of the particles, and the location of vanishing relative velocity moves away from the wall by decreasing the mass loading ratio.
3. Significant reduction of the fluid turbulent shear stress occurs due to the dissipating effects of the particles. This is accompanied by a decrease in the turbulent kinetic energy of the fluid.
4. For the same mean-flow Reynolds number, a more powerful pump is needed for pumping a gas–solid suspension in a vertical pipe than is required for pumping gas alone.
5. The predicted modification of the law-of-the-wall by the particles suggests that the use of the single-phase law-of-the-wall for two-phase flows is an inaccurate representation of the real situation for volumetric loading ratios >0.0005.

REFERENCES

AL TAWEEL, A. M. & LANDAU, J. 1977 Turbulence modulation in two-phase jets. *Int. J. Multiphase Flow* **3,** 341–351.

BRENNER, H. 1961 The slow motion of a sphere through a viscous fluid towards a plane surface. *Chem. Engng Sci.* **16,** 242–251.

CHIEN, K. Y. 1980 Prediction of channel and boundary layer flow with a low-Reynolds-number two-equation model of turbulence. AIAA Paper 80-0134.

CHOI, Y. D. & CHUNG, M. K. 1983 Analysis of turbulent gas–solid suspension flow in a pipe. *ASME Jl Fluids Engng* **105,** 329–334.

CLIFT, R., GRACE, J. R. & WEBER, M. E. 1978 *Bubbles, Drops and Particles.* Academic Press, New York.

CSANADY, G. T. 1963 Turbulent diffusion of heavy particles in the atmosphere. *J. atmos. Sci.* **20,** 201–208.

DREW, D. A. 1975 Turbulent sediment over a flat bottom using momentum balance. *J. appl. mech.* **97,** 38–44.

ELGHOBASHI, S. E. & ABOU-ARAB, T. W. 1983 A two-equation turbulence model for two-phase flows. *Phys. Fluids* **26,** 931–938.

ELGHOBASHI, S., ABOU-ARAB, T., RIZK, M. & MOSTAFA, A. 1984 Prediction of the particle-laden jet with a two-equation turbulence model. *Int. J. Multiphase Flow* **10,** 697–710.

FAXEN, H. 1923 *Ark. Mat. Astr. Fys.* **17,** 1.

GOUESBET, G., BERLEMEONT, A. & PICART, A. 1983 Miscellaneous problems and results connected with the improvements and applications of the code DISCO-2 for the prediction of the behaviour of discrete particles in turbulent flows. Internal Report NADO/GPB/1/83/I, Faculte' des Sciences de Rouen, France.

HINZE, J. O. 1975 *Turbulence.* McGraw-Hill, New York.

JONES, W. P. & LAUNDER, B. E. 1972 the prediction of laminarization with a two-equation model of turbulence. *Int. J. Heat Mass Transfer* **15,** 301–314.

KRAMER, T. J. & DEPEW, C. A. 1972 Analysis of mean flow characteristics of gas–solids suspensions. *J. basic Engng* **94,** 731–738.

LAUFER, J. 1954 The structure of turbulence in fully developed pipe flow. NACA Report 1174, pp. 417–434.

LAUNDER, B. E. & SPALDING, D. B. 1972 *Mathematical Models of Turbulence.* Academic Press, London and New York.

MAEDA, M., HISHIDA, K. & FURUTANI, T. 1980 Optical measurements of local gas and particle velocity in an upward flowing dilute gas–solids suspension. In *Proc. Polyphase Flow and Transport Technology*, p. 211. Century 2-ETC, San Francisco, Calif.

MAUDE, A. D. 1961 End effects in a falling-sphere viscometer. *Br. J. appl. Phys.* **12,** 293–295.

MODARRESS, D., WUERER, J. & ELGHOBASHI, S. 1984 An experimental study of a turbulent round two-phase jet. *Chem. Engng Commun.* **28,** 341–354.

MODARRESS, D., TAN, H. & ELGHOBASHI, S. 1984 Two-component LDA measurement in a two-phase turbulent jet. *AIAA Jl* **22,** 624–630.

OWEN, P. R. 1969 Pneumatic transport. *J. Fluid Mech.* **39,** 407–432.

POURAHMADI, F. & HUMPHREY, J. A. C. 1983 Modeling solid–fluid turbulent flows with application to predicting erosive wear. *PhysicoChem. Hydrodynam.* **4,** 191–219.

RIZK, M. A. 1985 A two-equation turbulence model for free and bounded two-phase flows. Ph.D. Thesis, Univ. of California, Irvine.

RIZK, M. A. & ELGHOBASHI, S. E. 1985 On the motion of a spherical particle suspended in a turbulent flow near a plane wall. *Phys. Fluids* **28,** 806–817.

RODI, W. 1980 *Turbulence Models and their Applications in Hydraulics.* International Associate for Hydraulic Research, Delft, The Netherlands.

SAFFMAN, P. G. 1962 On the stability of laminar flow of a dusty gas. *J. Fluid Mech.* **13,** 120.

SAFFMAN, P. G. 1965 The lift on a small sphere in a slow shear flow. *J. Fluid Mech.* **22,** 385–400.

SAFFMAN, P. G. 1968 Corrigendum. *J. Fluid Mech.* **31,** 624.

SNYDER, W. H. & LUMLEY, J. L. 1971 Some measurements of particle velocity autocorrelation functions in a turbulent flow. *J. Fluid Mech.* **48,** 1.

SPALDING, D. B. 1979 Numerical computation of multiphase flows. Lecture Notes, Thermal Science and Propulsion Center, Purdue Univ., Lafayette, Ind.

THEODORE, L. 1964 Sidewise force exerted on a spherical particle in a Poiseuillian flow field. Engng Sci. D. Dissertation, New York Univ., N.Y.

TSUJI, Y., MORIKAWA, Y. & SHIOMI, H. 1984 LDV measurements of an air–solid two-phase flow in a vertical pipe. *J. Fluid Mech.* **139,** 417–434.

WELLS, M. W. 1982 The effects of crossing trajectories on diffusion of particles in a turbulent fluid. Ph.D., Washington State Univ., Pullman, Wash.

ZISSELMAR, R. & MOLERUS, O. 1979 Investigation of solid–liquid pipe flow with regard to turbulence modification. *Chem. Engng J.* **18,** 233.